The Journal of Chemical Physics

Broadband adiabatic inversion experiments for the measurement of longitudinal relaxation time constants

Cite as: J. Chem. Phys. **154**, 034202 (2021); https://doi.org/10.1063/5.0039017
Submitted: 29 November 2020 . Accepted: 17 December 2020 . Published Online: 21 January 2021

Adam R. Altenhof, Michael J. Jaroszewicz, Kristopher J. Harris, and Robert W. Schurko

The Journal of Chemical Physics ARTICLE scitation.org/journal/jcp

Broadband adiabatic inversion experiments for the measurement of longitudinal relaxation time constants

Cite as: J. Chem. Phys. 154, 034202 (2021); doi: 10.1063/5.0039017
Submitted: 29 November 2020 • Accepted: 17 December 2020 •
Published Online: 21 January 2021

Adam R. Altenhof,[1,2] Michael J. Jaroszewicz,[3,a)] Kristopher J. Harris,[4] and Robert W. Schurko[1,2,b)]

AFFILIATIONS

[1]National High Magnetic Field Laboratory, 1800 East Paul Dirac Drive, Tallahassee, Florida 32310, USA
[2]Department of Chemistry and Biochemistry, Florida State University, Tallahassee, Florida 32306, USA
[3]Department of Chemistry and Biochemistry, University of Windsor, Windsor, Ontario N9B 3P4, Canada
[4]Department of Chemistry, Louisiana Tech University, Ruston, Louisiana 71272, USA

[a)]**Current address:** Department of Chemical and Biological Physics, Weizmann Institute of Science, Rehovot 76100, Israel.
[b)]**Author to whom correspondence should be addressed:** rschurko@fsu.edu. **Tel.:** (850)-645-8614

ABSTRACT

Accurate measurements of longitudinal relaxation time constants (T_1) in solid-state nuclear magnetic resonance (SSNMR) experiments are important for the study of molecular-level structure and dynamics. Such measurements are often made under magic-angle spinning conditions; however, there are numerous instances where they must be made on stationary samples, which often give rise to broad powder patterns arising from large anisotropic NMR interactions. In this work, we explore the use of wideband uniform-rate smooth-truncation pulses for the measurement of T_1 constants. Two experiments are introduced: (i) BRAIN-CPT1, a modification of the BRAIN-CP (BRoadband Adiabatic-INversion-Cross Polarization) sequence, for broadband CP-based T_1 measurements and (ii) WCPMG-IR, a modification of the WURST-CPMG sequence, for direct-excitation (DE) inversion-recovery experiments. A series of T_1 constants are measured for spin-1/2 and quadrupolar nuclei with broad powder patterns, such as ^{119}Sn ($I = 1/2$), ^{35}Cl ($I = 3/2$), ^{2}H ($I = 1$), and ^{195}Pt ($I = 1/2$). High signal-to-noise spectra with uniform patterns can be obtained due to signal enhancements from T_2^{eff}-weighted echo trains, and in favorable cases, BRAIN-CPT1 allows for the rapid measurement of T_1 in comparison to DE experiments. Protocols for spectral acquisition, processing, and analysis of relaxation data are discussed. In most cases, relaxation behavior can be modeled with either monoexponential or biexponential functions based upon measurements of integrated powder pattern intensity; however, it is also demonstrated that one must interpret such T_1 values with caution, as demonstrated by measurements of T_1 anisotropy in ^{119}Sn, ^{2}H, and ^{195}Pt NMR spectra.

I. INTRODUCTION

Solid-state nuclear magnetic resonance (SSNMR) is a powerful tool for elucidating information on molecular-level structure and dynamics. SSNMR relies primarily upon the measurements of secular effects in spectra, such as shifts and splittings, in order to gain information about NMR interaction tensors; in turn, these provide information on local chemical environments, internuclear distances, long-range order, dynamical processes, and/or chemical exchange. All of the NMR interactions have the potential to contribute to non-secular effects arising from nuclear magnetic relaxation phenomena, which are commonly described by means of relaxation time constants, such as the longitudinal (T_1), transverse (T_2), and spin-locking ($T_{1\rho}$) time constants. Knowledge of the relaxation time constants is crucial not only for the proper and efficient execution of NMR experiments but also for further elucidation of structure and dynamics.[1–3]

The accurate measurement of relaxation time constants can be challenging due to the low intrinsic sensitivity of the NMR experiment. For instance, the measurement of long T_1 relaxation

times can be very time consuming in situations where signal-to-noise (S/N) is low; this can be especially arduous when conducting measurements on nuclei with low gyromagnetic ratios (γ), low natural abundances (n.a.) or concentrations, and/or large anisotropic interactions.[4] The latter generally result in significant inhomogeneous broadening of spectra and may arise from chemical shift anisotropy (CSA), the first-order quadrupolar interaction (FOQI), the second-order quadrupolar interaction (SOQI), dipolar broadening, paramagnetic broadening, Knight shift anisotropy, and potentially any combinations of these. The contributions from these interactions to relaxation can also be anisotropic such that relaxation time constants can vary for different orientations of the interaction tensor(s) with respect to the magnetic field.[1,5–8] All of these factors are exceptionally problematic for measurements of lengthy T_1 constants of heavy spin-1/2 nuclei, such as ^{119}Sn, ^{195}Pt, ^{199}Hg, and ^{207}Pb,[9–15] and of many quadrupolar (spin >1/2) nuclei, such as ^{2}H, ^{6}Li, ^{10}B, ^{14}N, ^{17}O, ^{23}Na, ^{27}Al, ^{35}Cl, and others, which may have long T_1 values due to small quadrupolar interactions resulting from a small to moderate nuclear quadrupole moment (eQ) and/or a reduced quadrupolar coupling constant (C_Q).

Several techniques have been introduced to improve the efficiency of longitudinal relaxation measurements in SSNMR experiments, most of which are conducted under magic-angle spinning (MAS) conditions to average anisotropic interactions. Cross polarization (CP)/MAS is traditionally used for enhancing sensitivity, and variations of this sequence have been widely applied for measuring the T_1 of spin-1/2 nuclei (e.g., ^{13}C) in organic solids.[16–22] Many researchers have also used T_1 measurements in ^{2}H SSNMR studies of molecular dynamics; such measurements are typically made on stationary (static) samples.[7,23–27] The CPT1 pulse sequence of Torchia is the standard method for measuring T_1's of the dilute S spin with CP/MAS (i.e., for an IS spin system).[28] This sequence has the benefit of acquiring CP-enhanced S-spin spectra while simultaneously suppressing artifacts originating from non-CP polarization, pulse breakthrough, and/or acoustic ringing.[29] In cases where $T_1(I) < T_1(S)$, a significant reduction in experimental time can be achieved over non-CP methods. For CP-based sequences, careful consideration must be given to heteronuclear dipolar coupling as a source of cross relaxation, which can lead to nonexponential decay associated with time constants $T_1(IS)$ and $T_1(SI)$.[12,23,30] McDowell *et al.* addressed this issue and noted that these effects do not manifest when $T_1(S)$ is sufficiently longer than $T_1(I)$.[16,18] For direct-excitation (DE) measurements of $T_1(S)$ (i.e., often in the cases of ^{13}C and ^{2}H experiments), standard saturation recovery (SR) or inversion recovery (IR) is used instead, where IR is generally regarded as a more accurate means of measuring T_1.[5,17] Yesinowski has described methods for measuring T_1 constants by direct excitation and detection of half-integer spin quadrupolar nuclei under both static and MAS conditions, giving careful consideration to contributions from satellite transitions, which can also manifest multiexponential decay behavior.[31,32] Venkatesh *et al.* have used indirectly detected D-RINEPT under fast MAS for measuring T_1's of half-integer quadrupolar nuclei (HIQN).[33] Finally, Makrinich and Goldbourt recently implemented an indirectly detected CP-MAS SR technique for measuring T_1's of quadrupoles, such as ^{14}N.[34]

Many nuclei from elements across the periodic table experience large anisotropic interactions that result in powder patterns ranging from hundreds of kHz to several MHz in breadth. We have defined ultra-wideline (UW) NMR spectra as those with patterns spanning over 250 kHz in breadth[35] since we have empirically observed that it is not generally possible to excite, refocus, and acquire uniform patterns using conventional rectangular pulses and techniques using standard coil sizes (e.g., 3.2 mm and larger);[4] rather, acquisition of uniform, high-quality, UWNMR patterns often requires specialized pulse sequences and/or hardware, frequency-stepped/field-swept acquisitions, increased magnetic field strengths, fast or ultra-fast MAS, and even combinations of these techniques in certain cases.[35] We note that MAS methods are generally not useful for most half-integer quadrupolar nuclei experiencing large quadrupolar interactions that give rise to UWNMR spectra since it is not possible to average the effects of the second-order quadrupolar interaction, and high-resolution techniques like multiple-quantum MAS (MQMAS) and satellite-transition MAS (STMAS) are hampered by severe overlap of the isotropic and sideband patterns.[36,37]

Two techniques that are well established for acquiring UWNMR spectra for stationary samples are the WURST-CPMG (WCPMG) and BRAIN-CP/WURST-CPMG (BRAIN-CP) pulse sequences.[38,39] Both sequences employ frequency-swept (FS) wideband uniform-rate smooth-truncation (WURST) pulses for excitation, refocusing, and/or polarization transfer over broad bandwidths[40] and Carr–Purcell–Meiboom–Gill (CPMG)-type sequences for signal enhancement.[41–44] It should be noted that the BRAIN-CP FS pulse must be long enough to allow the adiabatic passage of polarization, while the FS pulse used for echo generation is generally a rapid sweep that the spin polarization follows reproducibly and coherently, but not adiabatically.[45] These sequences have intrinsic features that may lend themselves to be useful for relaxation measurements. For instance, WCPMG has been used to measure effective T_2's (T_2^{eff}s) in UWNMR patterns of spin-1/2 and quadrupolar nuclei from the CPMG echo trains,[46,47] and DE with WURST pulses has been used for the inversion of spin polarization in UWNMR experiments.[47] I–S BRAIN-CP uses a WURST pulse for adiabatic inversion of dilute S-spin polarization during the CP contact period.[39,48] Therefore, the magnetization is already in the z-direction at the end of the CP process, allowing longitudinal relaxation to propagate without needing the flip-back pulses used by Torchia.[28] Accordingly, BRAIN-CP is naturally adapted for measuring $T_1(S)$ constants in static-sample UWNMR powder patterns. Since the efficiency of BRAIN-CP, in part, depends on the spin polarization of ^{1}H at thermal equilibrium and $T_1(^{1}\text{H})$ relaxation times can be short in comparison to those of the S nuclei with UWNMR patterns, there is potential to measure long T_1 values of rare S-spins while only having to wait for the ^{1}H-spin polarization to return to thermal equilibrium between scans. Furthermore, significant signal enhancement can be gained from CP (especially for low-γ nuclei), allowing for even faster measurements of T_1. If CP is inefficient or not possible, it is feasible to design an experiment using a DE WURST pulse that inverts the S-spin polarization. Finally, a potential benefit in both DE and CP experiments of this nature is signal enhancement from the CPMG T_2^{eff}-weighted echo train, which can also present opportunities for the accurate measurements of T_2^{eff}.

Herein, we present two experiments, BRAIN-CPT1 and WCPMG-IR (Scheme 1), and demonstrate them as efficient and reliable methods for measuring T_1 time constants of nuclei with broad powder patterns under static conditions. Careful consideration is given to the proper implementation of these sequences, which can

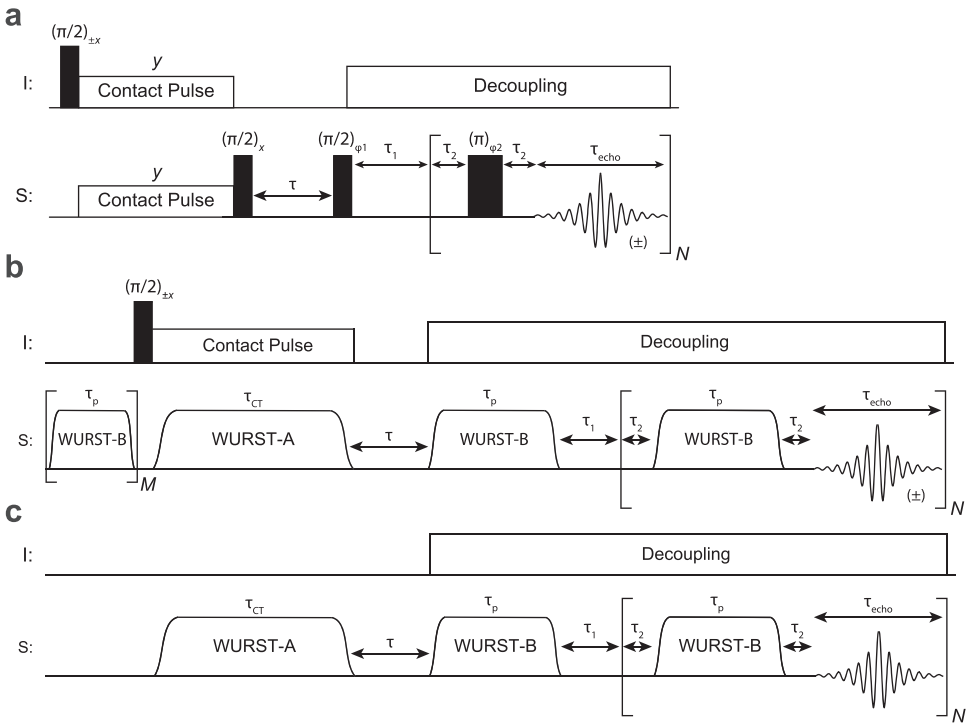

SCHEME 1. (a) The CP-CPMGT1 pulse sequence utilizing pulses of constant amplitude and phase, (b) the BRAIN-CPT1 pulse sequence, and (c) the WCPMG-IR pulse sequence. The delay time, τ, is incremented in every case. In (a) and (b), the phase of the ^{1}H excitation pulse controls whether the signal is stored as $\pm S_z$ during τ; this can also vary depending on the WURST-A sweep direction in (b). These details are further described in the main text.

vary depending on the dominant NMR interaction(s) (i.e., CSA, FOQI, or SOQI). Examples are discussed for T_1 measurements on systems with ^{119}Sn, ^{35}Cl, ^{2}H, and ^{195}Pt nuclei, such as a comparison of mean T_1 values obtained from integrated powder patterns with those obtained by measuring T_1 as a function of isochromat frequency (i.e., T_1 anisotropy).

II. EXPERIMENTAL

A. Samples

Dibutyltin(IV) oxide (Sigma Aldrich), glycine HCl (Sigma Aldrich), partially deuterated α-glycine (α-glycine-d_2, Cambridge Isotope Laboratories, Inc.), and tetraammineplatinum(II) chloride monohydrate [$Pt(NH_3)_4Cl_2{\cdot}H_2O$, Sigma Aldrich] were purchased and used in all subsequent NMR experiments without further purification. The identities and purities of the samples were verified through comparisons with previously reported NMR spectra and PXRD patterns.[11,48–50] All samples were ground into fine powders and packed into 5 mm outer-diameter glass tubes that were sealed with Teflon tape.

B. Solid-state NMR spectroscopy

NMR spectra were acquired using a Bruker Avance NEO console and a 14.1 T Magnex/Bruker [$\upsilon_0(^1H)$ = 600 MHz] wide-bore magnet at resonance frequencies of $\upsilon_0(^{119}Sn)$ = 223.77 MHz, $\upsilon_0(^{35}Cl)$ = 58.787 MHz, $\upsilon_0(^2H)$ = 92.104 MHz, and $\upsilon_0(^{195}Pt)$ = 128.981 MHz. A home-built 5 mm double-resonance (HX) probe was used for all experiments. All data were collected under static conditions (i.e., stationary samples). Spectra were acquired with ^{1}H continuous-wave (CW) decoupling with RF fields of 50 kHz. RF pulse powers and chemical-shift reference frequencies were calibrated using the following standards: (i) ^{119}Sn reference: $Sn(CH_3)_4$ (*l*) with δ_{iso} = 0.0 ppm, (ii) ^{35}Cl reference: NaCl (*s*) with δ_{iso} = 0.0 ppm, (iii) ^{2}H reference: D_2O (*l*) with δ_{iso} = 4.8 ppm, and (iv) ^{195}Pt reference: 1.0 M Na_2PtCl_6 (*aq*) with δ_{iso} = 0.0 ppm.

C. Spectral processing

All datasets were processed and fit in MATLAB using a custom-written code. For each relaxation data point, each of which is denoted by the delay, τ (see Scheme 1), the NMR signal, in the form of multiple spin echoes, is acquired with a CPMG-type echo train featuring WURST refocusing pulses. These echoes are coadded into a single echo, Fourier transformed, and then phase-corrected with zeroth, first, and second-order phasing;[43] hence, each spectrum utilized in the T_1-fitting routine is the result of the co-addition of the entire T_2^{eff}-weighted echo train. The resulting integrated intensity of the powder pattern for each relaxation data point is used for T_1 fitting. Thirty-two logarithmically sampled τ increments were measured in every experiment in this work. The data acquired with the BRAIN-CPT1 pulse sequence are fit with monoexponential and biexponential decay functions of the form $ae^{-\tau/T_{1a}} + be^{-\tau/T_{1b}}$ ($b = 0$ in the monoexponential case), and the data acquired with the WCPMG-IR pulse sequence are fit with $1 - ae^{-\tau/T_{1a}} - be^{-\tau/T_{1b}}$. In both cases, T_{1a} and T_{1b} describe the longer and shorter time constants, respectively. In some cases, the spectral intensity of each frequency in the powder pattern is fit as a function of the τ increment rather

than the integrated intensity across the powder pattern (*vide infra*). Numerical simulations were performed in SIMPSON 4.2.1.[51]

III. RESULTS AND DISCUSSION

A. Overview

In Secs. III B–III G, it is demonstrated that BRAIN-CPT1 and WCPMG-IR are suitable methods for measuring T_1 constants from static UWNMR spectra and are superior to methods utilizing pulses of constant phase and amplitude. To the best of our knowledge, there have been no reports of using T_2^{eff}-weighted echo trains from CPMG to conduct SSNMR T_1 measurements (Scheme 1). A simple modification of Torchia's CPT1 pulse sequence is shown in Scheme 1(a) (referred to as CP-CPMGT1), where a standard CPMG pulse sequence with rectangular pulses for CP and refocusing is used to acquire signals. For CP-based pulse sequences for measuring T_1, it is necessary to acquire two datasets originating from $+S_z$ and $-S_z$ spin polarization stored during τ and to subtract the latter dataset from the former in order to suppress unwanted signals from transverse *S*-spin polarization that does not arise from CP processes.[28] The relative sign of the spin polarization during τ can be controlled by the phase of the π/2 excitation pulse on the *I* channel [Schemes 1(a) and 1(b)].[29] BRAIN-CPT1 operates identically to standard BRAIN-CP,[48] but with the additional incremented τ delay time after the WURST-A pulse to allow for longitudinal relaxation to occur [Scheme 1(b)]. BRAIN-CPT1 initiates with a continuous train of WURST pulses to saturate *S*-spin polarization in order to further avoid unwanted non-CP polarization. WCPMG-IR operates similarly to BRAIN-CPT1, but without any excitation or spin-locking on the *I* channel, no pre-saturation pulses [Scheme 1(c)], and only requires only a single dataset (i.e., no pulse phase variation at the start of the sequence). The proper implementation of these sequences can vary depending on the dominant NMR interaction affecting relaxation (i.e., mechanisms arising from CSA, QI, dipolar interactions, and coupling with unpaired electrons) as well as the secular manifestation of the interactions. Resulting datasets are carefully analyzed with monoexponential and biexponential fitting of either the integrated powder patterns or the individual isochromat intensities as a function of the incremented delay time. Several examples are explored to demonstrate this, such as measurements of T_1 constants for ^{119}Sn (I = 1/2), ^{35}Cl (I = 3/2), ^{2}H (I = 1), and ^{195}Pt (I = 1/2).

B. ^{119}Sn experiments

The ^{119}Sn static NMR spectrum of dibutyltin(IV) oxide exhibits a broad powder pattern with a breadth of ~170 kHz at 14.1 T [ideal

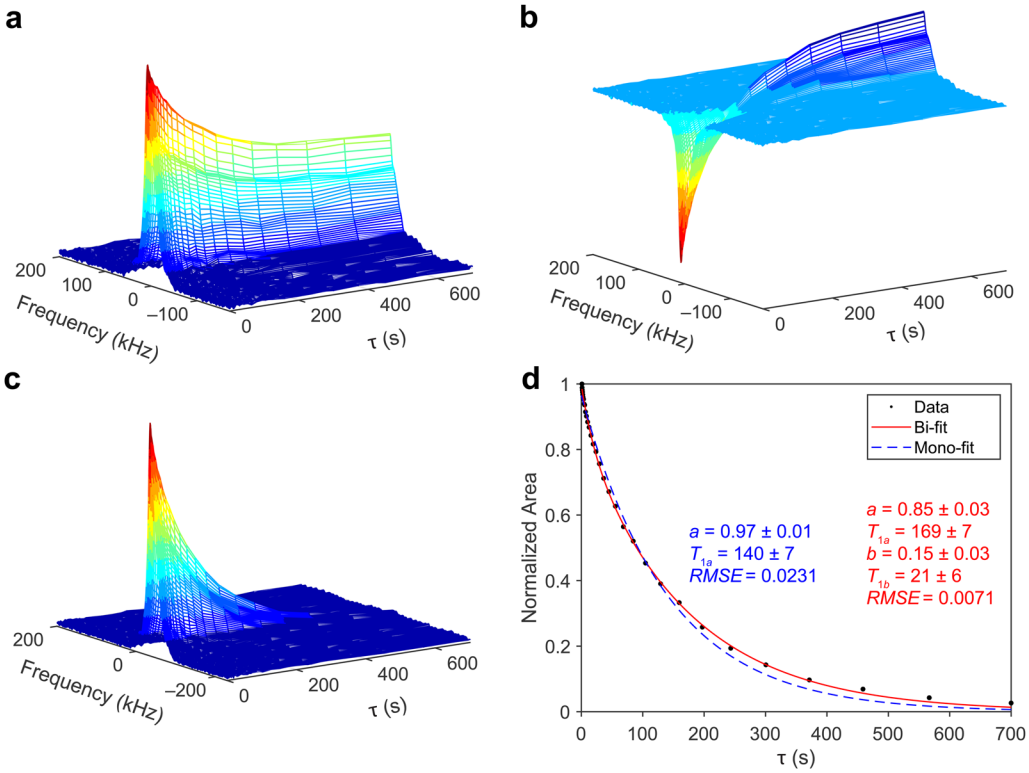

FIG. 1. ^{119}Sn NMR spectra of dibutyltin(IV) oxide acquired with the CP-CPMGT1 pulse sequence (a) using a phase of *x* for the ^{1}H π/2 excitation pulse and (b) using a phase of −*x*. (c) The difference between the datasets in (a) and (b). (d) Corresponding normalized integrated areas under the powder pattern as a function of the delay time τ with the fitted monoexponential and biexponential functions.

pattern shown in Fig. S1(a)] and is used as a test sample in this study (this compound was previously studied by our group for the development of the BRAIN-CP pulse sequence).[48] ^{1}H–^{119}Sn CP experiments on dibutyltin(IV) oxide are much faster in comparison to those where the ^{119}Sn nucleus is excited directly. For instance, the full sets of CP-CPMGT1 and BRAIN-CPT1 experiments each took ~9.5 h to complete due to the relatively short recycle delay of 20 s that is dependent on $T_1(^{1}\mathrm{H})$. A single IR experiment featuring DE of ^{119}Sn with the same number of scans would take ~29 h due to the substantially longer $T_1(^{119}\mathrm{Sn})$ and accordingly longer recycle delay of ~700 s (*N.B.*: If a DE IR experiment was run for the same number of scans, the resulting spectra would be lower in S/N due to the lack of CP enhancement, requiring more scans to compensate for this and resulting in experimental times significantly longer than 29 h).

The $T_1(^{119}\mathrm{Sn})$ measurement was first conducted using the CP-CPMGT1 pulse sequence consisting only of rectangular pulses. This first requires acquisition with the x-phase shifted ^{1}H excitation pulse [Fig. 1(a)]. After the CP step, S-spin polarization is parallel with the spin-locking pulse in the xy-plane; therefore, a $\pi/2$ pulse is needed to flip magnetization to $+S_z$. After some delay time, τ, a standard CPMG pulse sequence is executed to detect the magnetization; this is done for each τ-increment (32 logarithmically spaced τ points are used). The data are processed as described in Sec. II (*vide supra*). An identical experiment is executed, save for the phase of the ^{1}H excitation pulse, which now has a relative phase shift of $-x$, causing the spin polarization to be stored as $-S_z$ during τ [Fig. 1(b)]. The difference between the datasets is then taken as $+S_z - [-S_z]$ [Fig. 1(c)]. The resulting CP-CPMGT1 data were fit with monoexponential and biexponential functions; however, slightly better fits were obtained with the latter [Fig. 1(d) and Table I], which yields values of T_{1a} = 169 ± 7 s and T_{1b} = 21 ± 6 s. The relative weights of the first and second terms are a = 0.85 ± 0.03 and b = 0.15 ± 0.03, respectively, indicating a larger contribution from T_{1a}. High quality fits are obtained, as indicated by the root-mean-square error (*RMSE*) values near 0, but the spectra are non-uniform in comparison to the ideal pattern due to insufficiently broadband CP-enhancement and refocusing across the bandwidth of the pattern (Fig. S2, *vide infra*).

Before attempting measurements of $T_1(^{119}\mathrm{Sn})$ using the BRAIN-CPT1 sequence, careful consideration was given to the choice of relative phases for the ^{1}H excitation pulse and the *sweep direction* of the BRAIN (WURST-A) pulse on the S channel since this determines if spin polarization is generated as $+S_z$ or $-S_z$. For a ^{1}H $\pi/2$ pulse with phase $\pm x$ and a BRAIN contact pulse that sweeps from high-to-low frequency, polarization is stored as $\pm S_z$ during τ, which is identical to the behavior of spin polarization under the CP-CPMGT1 sequence. If instead the BRAIN pulse sweeps from low-to-high frequency [with the same initial $(\pi/2)_{\pm x}$ pulse on ^{1}H], polarization is stored as $\mp S_z$ (i.e., opposite in sign to the first case).[48] For ^{119}Sn experiments herein, the BRAIN pulse is always swept from high-to-low frequency.

BRAIN-CP can transfer polarization uniformly across the entire frequency range of this powder pattern, and WCPMG can efficiently excite and refocus the spin polarization for detection (Fig. 2). CP-CPMG is able to enhance the S-spin polarization; however, the rectangular pulses on the S channel are inherently bandwidth limited for excitation, refocusing, and especially during CP (Fig. S2).[48] As such, the CP-CPMGT1 pulse sequence may be unsuitable for most experiments on broader UWNMR patterns and is not recommended for use in UWNMR experiments.

BRAIN-CPT1 is conducted with a ^{1}H excitation pulse phase of $+x$ [Fig. 2(a)] and $-x$ [Fig. 2(b)], and the difference between the two resulting datasets is taken [Fig. 2(c)]. The resulting fit yields values of T_{1a} = 159 ± 5 s and T_{1b} = 20 ± 5 s [Fig. 2(d)] and weights of a = 0.84 ± 0.02 and b = 0.15 ± 0.02, respectively, which differs slightly from the CP-CPMGT1 measurement but does agree within the bounds of uncertainty (Table I). The BRAIN-CPT1 experiment results in a powder pattern that matches well with ideal simulations due to uniform excitation and refocusing of spin polarization and is therefore a more reliable measure of T_1. Similar results can be obtained using a single dataset derived from an initial $-x$ pulse and storage

TABLE I. Monoexponential and biexponential fits of T_1 data obtained from pattern integration.

Sample	Experiment	a	T_{1a} (s)	b	T_{1b} (s)	*RMSE*
Dibutyltin(IV) oxide (^{119}Sn)	CP-CPMGT1	0.97 ± 0.01	140 ± 7	. . .	. . .	0.0231
	CP-CPMGT1	0.85 ± 0.03	169 ± 7	0.15 ± 0.03	21 ± 6	0.0071
	BRAIN-CPT1	0.96 ± 0.01	131 ± 7	. . .	. . .	0.0228
	BRAIN-CPT1	0.84 ± 0.02	159 ± 5	0.15 ± 0.02	20 ± 5	0.0057
Glycine HCl (^{35}Cl)	BRAIN-CPT1	0.989 ± 0.008	0.187 ± 0.006	. . .	. . .	0.0137
	BRAIN-CPT1	0.52 ± 0.07	0.290 ± 0.02	0.48 ± 0.07	0.109 ± 0.009	0.0022
	WCPMG-IR	1.98 ± 0.01	0.210 ± 0.007	. . .	. . .	0.0266
	WCPMG-IR	1.19 ± 0.08	0.310 ± 0.01	0.81 ± 0.08	0.113 ± 0.006	0.0024
α-Glycine-d_2 (^{2}H)	BRAIN-CPT1 LtoH[a]	1.02 ± 0.02	20.1 ± 0.9	. . .	. . .	0.0208
	BRAIN-CPT1 LtoH[a]	0.53 ± 0.03	33 ± 1	0.52 ± 0.07	10.4 ± 0.5	0.0017
	BRAIN-CPT1 HtoL[a]	1.03 ± 0.02	20.4 ± 0.9	. . .	. . .	0.0197
	BRAIN-CPT1 HtoL[a]	0.55 ± 0.02	32.6 ± 0.8	0.51 ± 0.02	10.7 ± 0.3	0.0011

[a]The frequency sweep direction of every WURST pulse in the BRAIN-CPT1 sequence is set as either low-to-high frequency (LtoH) or high-to-low frequency (HtoL).

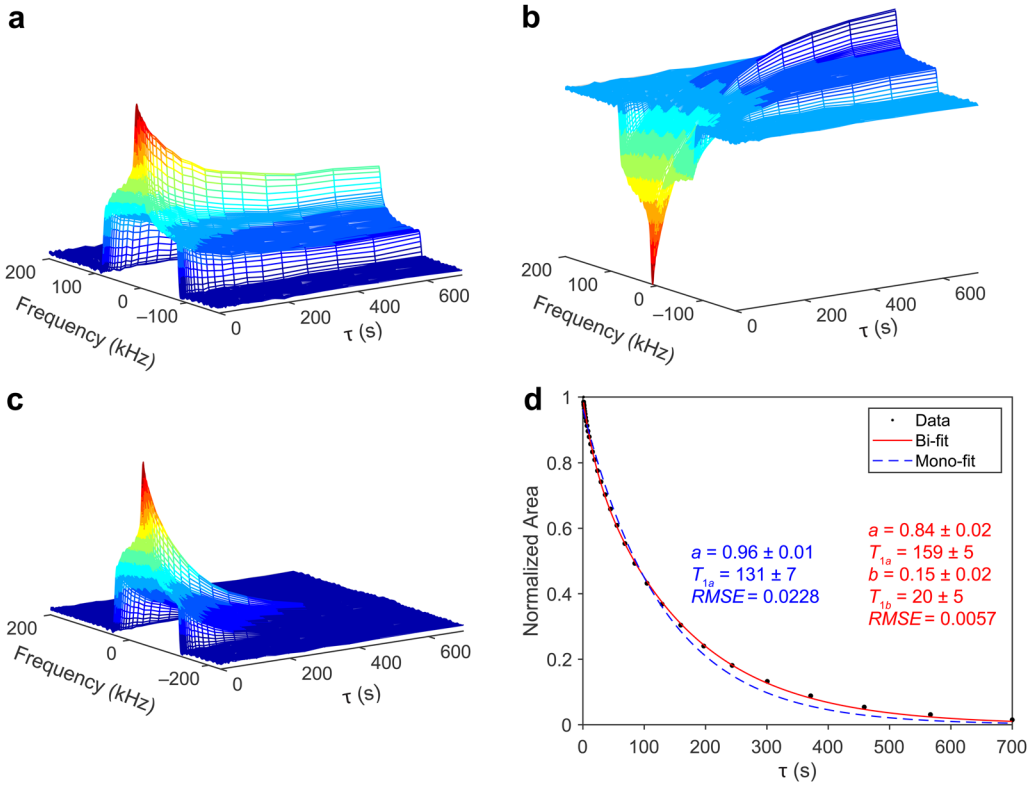

FIG. 2. ^{119}Sn NMR spectra of dibutyltin(IV) oxide acquired with the BRAIN-CPT1 pulse sequence (a) using a phase of x for the ^{1}H $\pi/2$ excitation pulse and (b) using a phase of $-x$. (c) The difference between the datasets in (a) and (b). (d) Corresponding normalized integrated areas under the powder pattern as a function of the delay time τ with the fitted monoexponential and biexponential functions. All WURST pulses are sweeping from high-to-low frequency.

of spin polarization as $-S_z$ since the pre-saturation guarantees that non-CP magnetization does not arise at the start of τ (cf. Fig. S3 for an explicit test of pre-saturation with ^{35}Cl NMR and Fig. S4 for an example of fitting a single dataset with the current ^{119}Sn example). This latter approach is twice as fast and produces very similar results; however, for purposes of comparison and consistency in the present work, the data are presented in all cases as two [$\pm S_z$ storage] datasets.

Biexponential modeling of the relaxation is observed to have a higher correlation with experimental data than monoexponential modeling with the *RMSE* values indicating that both are high quality fits. Examples of biexponential relaxation behavior were previously observed from measurements of $T_1(^{13}C)$.[16,17,52] For CP-based sequences, significant I_x polarization exists during the τ delays, which can introduce multiple cross relaxation terms. In order to observe only exponential decay, the I-spin pool must be saturated during the delay time τ. McDowell *et al.* noted the impracticality of decoupling on the I-channel when measuring long $T_1(S)$'s, which necessitates long τ delays (as long as 700 s in the present work). However, they note that for $T_1(S)$ values sufficiently longer than $T_1(I)$, these cross relaxation terms do not contribute and only monoexponential decay is observed, even without saturating the I spins.[16] In the present work, there is a small contribution from a term describing a fast T_{1b} process, whose inclusion does provide a better fit; however, the origin of the contributing relaxation mechanism is unclear (*N.B.*: Only likely contributing relaxation mechanisms arise from anisotropic dipolar and chemical shift interactions). We note that in our review of the literature describing the measurement of relaxation time constants in solids, there are numerous instances where only monoexponential relaxation processes are reported for a variety of different nuclei and materials. In many cases, this seems to be due to the absence of high-quality NMR data that would enable observation and measurement of the biexponential relaxation, the lack of logarithmically sampled τ increments to measure fast decays, and/or for the sufficiently high correlation of monoexponential fits. An investigation into the contributing mechanisms in biexponential relaxation behavior is currently underway in our research group.

It is important to note that it is possible to simultaneously extract high quality T_1 and T_2^{eff} measurements using BRAIN-CPT1 or WCPMG-IR. A preliminary foray into making these measurements is discussed in the supplementary material (see Table S1, Fig. S5, and the accompanying discussion); however, a detailed discussion of T_2^{eff} measurements and mechanisms is beyond the scope of the current work.

C. ^{35}Cl experiments

Glycine HCl is an excellent test sample for DE and CP experiments with a broad powder pattern of ~145 kHz at 14.1 T [ideal pattern shown in Fig. S1(b)]. ^{1}H and ^{35}Cl have short T_1's, allowing short recycle delays for this sample (2 s and 3 s, respectively), which enables the measurement of T_1 with both BRAIN-CPT1 and WCPMG-IR.[53,54] Interestingly, the signal enhancement from BRAIN-CP allows the experiment to be run much faster than the DE WCPMG-IR experiment (i.e., 40 min for the former and 114 min for the latter) in order to obtain spectra of similar S/N. The ^{1}H–^{35}Cl BRAIN-CPT1 experiment yields high S/N, CP-enhanced powder patterns that are uniform in appearance [Fig. 3(a)]. The BRAIN-CPT1 data are processed as described for ^{119}Sn experiments [i.e., the difference is taken between the two datasets originating from $\pm S_z$ polarization] and yield a fit of T_{1a} = 290 ± 20 ms and T_{1b} = 109 ± 9 ms. Biexponential fits again provide a slightly better match with experimental data in comparison to monoexponential fits [Fig. 3(c)]; however, there is an approximately equal contribution from both terms with $a = 0.52 \pm 0.07$ and $b = 0.48 \pm 0.07$.

The WCPMG-IR experiment operates in a similar manner to BRAIN-CPT1, with identical WURST-A pulses for inversion [Schemes 1(b) and 1(c)], but without the polarization enhancement from ^{1}H [Fig. 3(b)]. This means there are no potential artifacts from using CP or having residual ^{1}H polarization during τ; therefore, only one dataset is required, which can be modeled the same as a traditional DE IR experiment. The entire pattern is inverted uniformly, and the measurement is obtained with high S/N. The data are modeled with a biexponential decay function and yield T_{1a} = 310 ± 10 ms and T_{1b} = 113 ± 6 ms as well as relative weights of a and b that are in agreement with the BRAIN-CPT1 measurement (Table I). For monoexponential IR data, the pre-exponential factor should equal two; therefore, for the biexponential fit, the weights are normalized by a factor of two and are ca. $a = 0.6$ and $b = 0.4$, showing the agreement with BRAIN-CPT1 and again showing a slightly larger contribution from T_{1a}.

It is likely that there are at least two dominant relaxation processes since the relative weights of the T_1 terms are similar. Both values of T_1 are relatively small and are similar to $T_1(^{1}\text{H})$ in this case, which could allow cross relaxation terms to manifest;[16] however, since $\langle I_x \rangle \approx 0$ (i.e., no transverse ^{1}H spin polarization) during τ of the WCPMG-IR experiment, and this yields relaxation parameters that are close to those from the BRAIN-CPT1 measurement, it is unlikely that cross relaxation mechanisms are prevalent. It is possible that both dipolar and quadrupolar mechanisms contribute to relaxation in this case. Taylor *et al.* have shown that the $-NH_3^+$ group in

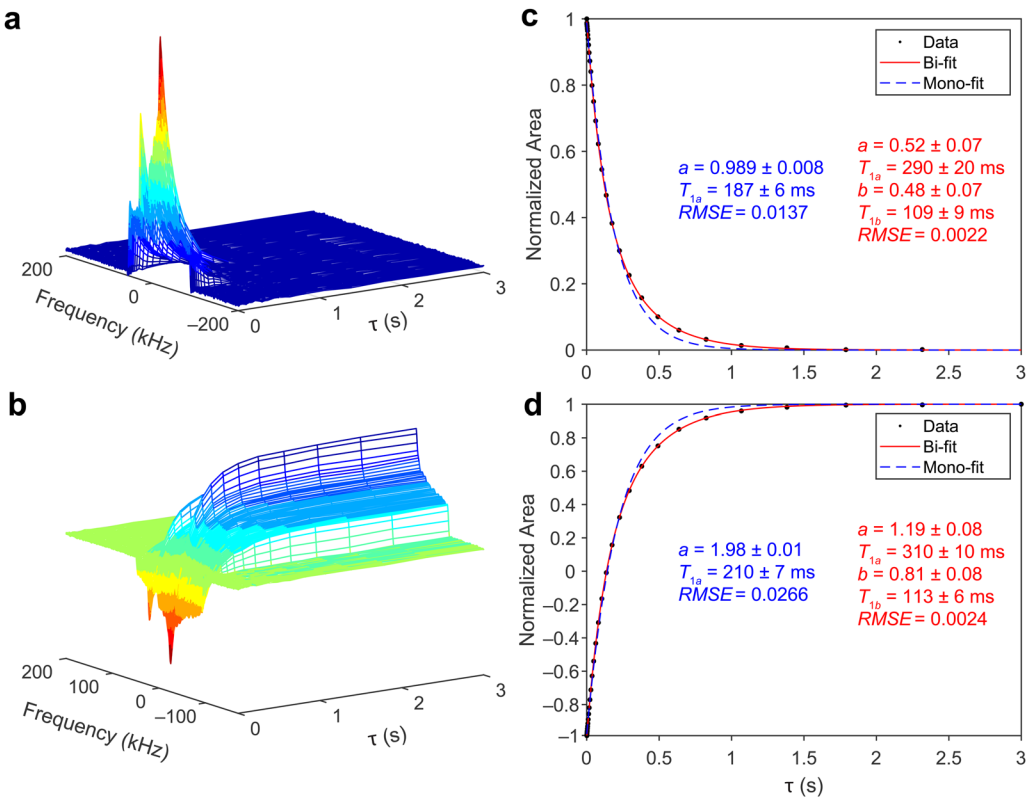

FIG. 3. ^{35}Cl NMR spectra of glycine HCl acquired with (a) the BRAIN-CPT1 and (b) WCPMG-IR pulse sequences. Corresponding normalized integrated areas under the powder pattern as a function of the delay time τ with the fitted monoexponential and biexponential functions are shown in (c) and (d).

γ-glycine drives dipolar relaxation for neighboring nuclei; therefore, it may be a source of dipolar relaxation for $T_1(^{35}\text{Cl})$ in glycine HCl.[24] Furthermore, in the case of CT spectra of half-integer quadrupolar nuclei (HIQN), where the QI can be a dominant contributor to relaxation, unique T_1 terms can originate from transition probabilities associated with both the single-quantum (SQ) satellite transitions (STs) and double-quantum (DQ) transitions. The combination of quadrupolar and dipolar relaxation mechanisms can give rise to up to three unique relaxation rates if T_1 is measured from thermal equilibrium. If quadrupolar relaxation is dominant, the observation of multiexponential decay is usually avoided by saturating the CT and STs before conducting the T_1 experiment.[31,32,34] In the current ^{35}Cl example, a saturation-recovery style pulse sequence yields a dataset that is also best fit with a biexponential function (Fig. S6). For static UWNMR spectra of HIQN, the powder patterns originating from the STs can often span several to tens of MHz, which is far beyond the excitation bandwidth of NMR probes and associated electronics. This makes it nearly impossible to completely saturate the STs, save for a few electric field gradient (EFG) crystallite orientations having frequencies that overlap with the CT region of the spectrum. It has been shown that WCPMG can intrinsically create MQCs by polarizing the STs for select crystallite orientations, and the creation of these MQCs is almost unavoidable.[55,56] Whether or not STs contribute to relaxation in this case is hard to deconvolute, but it is clear that $T_1(^{35}\text{Cl})$ for this sample has at least two contributing components, and further investigation into these phenomena is underway.

D. ^{2}H experiments

^{2}H is a spin-1 nucleus with two fundamental SQ transitions (i.e., $0 \longleftrightarrow \pm 1$). In solids, the orientation dependence of the FOQI results in two overlapping powder patterns that produce a Pake-like doublet [Fig. S1(c)]. Spin-1 nuclei pose an interesting case for both acquisition of spectra with BRAIN-CP and measuring T_1 with the BRAIN-CPT1 method. Our research group has demonstrated the utility of measuring static ^{14}N (also $I = 1$) powder patterns with BRAIN-CP.[39,57] We found that it is generally not possible to uniformly excite the entire pattern using ^{1}H–^{14}N BRAIN-CP; rather, specific regions of the pattern are selectively excited, depending upon the transmitter offset and BCP sequence parameters. There are three reasons for this: (i) Conventional CP to a spin-1 nucleus has two anisotropic Hartmann–Hahn (HH) matching conditions due to frequency shifts originating from the FOQI; therefore, the powder patterns originating from either shift cannot simultaneously be enhanced (using standard CP pulse sequences);[50,58] (ii) the BRAIN-CP HH matching conditions are time-dependent over the course of the frequency sweep and can have up to two matching conditions;[48,59] and (iii) population transfer and inversion take place when acquiring integer-spin NMR spectra with frequency-swept pulses, which typically results in the uniform acquisition of only one half of the Pake-like powder pattern.[60] For these reasons, BRAIN-CP acquisitions of static ^{2}H powder patterns need to be executed in a manner that accounts for these factors, resulting in the acquisition of just the high- or low-frequency half of the powder pattern in a single experiment (we refer to this as a *targeted acquisition*).[57] We note that for UWNMR patterns arising from large FOQI's, where the FOQI dominates the pattern and other anisotropic NMR interactions (e.g., CSA) may be neglected, it is only necessary to acquire one half of the Pake-like pattern for full characterization (one may also target selective sub-spectra with key discontinuities to further reduce experimental times).[57] Herein, our ^{1}H–^{2}H BRAIN-CPT1 experiments involve the separate acquisitions of both halves of the pattern with spectra acquired using both high-to-low and low-to-high frequency sweeps (Fig. S7).

α-Glycine-d_2 was used as a test sample, as it has a broad powder pattern of ~250 kHz. This sample has two magnetically inequivalent deuterons with very similar EFG tensor parameters;[61] therefore, their powder patterns are closely overlapped and are assumed to exhibit similar relaxation behavior [ideal pattern shown in Fig. S1(c)]. Müller *et al.* previously reported an upper bound of 210 s for $T_1(^2\text{H})$ of the $-\text{CD}_2$ group in α-glycine-d_5, and Takegoshi *et al.* estimated it to be ~45 s in α-glycine-d_2.[50,61] Each of the BRAIN-CPT1 experiments was completed in 284 min due to the short $T_1(^1\text{H})$, allowing a recycle delay of 2 s; analogous DE WCPMG-IR experiments would require ~13 h due to the recycle delay of ~150 s (*N.B.*: A DE IR experiment would have to signal average for more scans than the corresponding CP experiment in order to achieve the same level of S/N; therefore, such an experiment would exceed 13 h). The BRAIN-CPT1 experiment was first conducted on the high-frequency side of the powder pattern [Fig. 4(a)]. This necessitates that the transmitter offset frequency be set somewhere >0 kHz. This offset must be experimentally optimized for a given sample; in this case, an offset of +70 kHz maximizes the observable signal. All WURST pulses in the sequence must sweep from low-to-high frequency, and the phase of the ^{1}H excitation pulse must be varied as $\pm x$ to obtain two datasets from $\mp S_z$ spin polarization (see the discussion in the supplementary material). These conditions cause a population transfer and concomitant adiabatic inversion of S spin-polarization predominantly for isochromats on the high-frequency side of the powder pattern; therefore, only these isochromats undergo the exponential decays during the τ delay period that is suitable for measuring T_1. The difference is taken between the two datasets, and the area under the powder pattern is obtained by only integrating spectral regions >0 Hz [Fig. 4(c)]; fitting yields parameters of $T_{1a} = 33 \pm 1$ s and $T_{1b} = 10.4 \pm 0.5$ s. These terms have approximately equal weights with $a = 0.53 \pm 0.03$ and $b = 0.52 \pm 0.07$.

The same experiment was conducted on the low-frequency side of the powder pattern using the "opposite" pulse sequence parameters [Fig. 4(b)]. The transmitter frequency needs to be set somewhere < 0 kHz (in this case, −70 kHz was sufficient), all WURST pulses must sweep from high-to-low frequency, the phase of the ^{1}H excitation pulse must be varied as $\pm x$ to obtain two datasets from $\pm S_z$ spin polarization, and again, the difference is taken between these two datasets. In this case, spin polarization is only enhanced for isochromats on the low-frequency side of the pattern. Accordingly, a fit based on measurements of integrated intensities from the low-frequency half of the powder pattern yields values of $T_{1a} = 32.6 \pm 0.8$ s and $T_{1b} = 10.7 \pm 0.3$ s, and $a = 0.55 \pm 0.02$ and $b = 0.51 \pm 0.02$, which agrees well with the fit from the high-frequency side [Fig. 4(d)].

These results demonstrate that the relaxation characteristics are very similar for both halves of the ^{2}H powder pattern and, as such, can be measured using spectral intensities from only one half of the

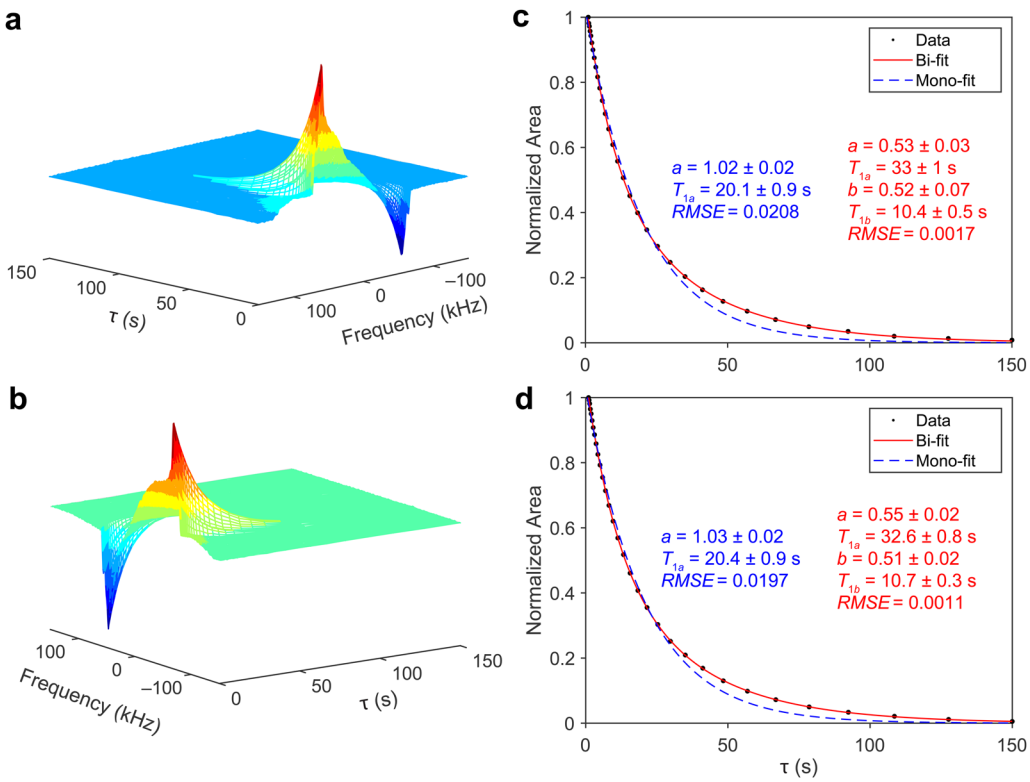

FIG. 4. ^{2}H NMR of α-glycine-d_2 acquired with the BRAIN-CPT1 pulse sequence (a) with the transmitter offset by ∼70 kHz with respect to $\nu_0(^2H)$ and all WURST pulses sweeping from low-to-high frequency and (b) with the transmitter offset by ∼−70 kHz with respect to $\nu_0(^2H)$ and all WURST pulses sweeping from high-to-low frequency. Corresponding normalized integrated areas under the (c) positive- and (d) negative-frequency halves of the respective powder patterns as a function of the delay time τ with the fitted monoexponential and biexponential functions shown. The plot in (b) is rotated by 90° with respect to (a) for visual clarity.

pattern. These same principles and techniques can easily be extended for T_1 measurements of ^{14}N. It is noted that care must be taken in cases where the pattern is asymmetric due to the influences of dipolar and/or paramagnetic interactions.

The origin of biexponential relaxation decay in α-glycine-d_2 can arise from both dipolar- and quadrupolar-driven relaxation mechanisms; however, based on previous reports on similar organic solids, the exact contributions from each are not clear. For instance, an interesting case study of a ^{2}H-labelled ethanol group in form C of formoterol fumarate was reported by Apperley *et al.*[23] Therein, they concluded that modulation of the quadrupolar interaction due to possible motion of the fumarate C–D bond is the dominant contributor to $T_1(^2H)$ relaxation, whereas a contribution to relaxation arising from ^{1}H–^{2}H dipolar interactions (with a neighboring methyl group) is minimal. In the case of γ-glycine, Dybowski *et al.* have shown that deuteration of the $-NH_3^+$ group significantly lengthens T_1 for nearby nuclei, such as ^{1}H, ^{13}C, and ^{15}N, confirming that the $-NH_3^+$ group can drive heteronuclear dipolar relaxation for neighboring nuclei. Unfortunately, an investigation into ^{2}H relaxation of the $-CD_2$ moiety was not presented. Hence, in α-glycine-d_2, it is feasible that the $-NH_3^+$ group might create dipolar modulations that contribute to $T_1(^2H)$ along with small amplitude motions of the $-CD_2$ group that cause modulations of the EFG tensor. If both dipolar and quadrupolar contributions to relaxation are present, this might account for the observed biexponential $T_1(^2H)$ behavior with approximately equal contributions from slow and fast processes. This is partially confirmed by $T_1(^2H)$ measurements of the $-CD_2$ group in α-glycine-d_5, where monoexponential fits yield $T_1(^2H)$ = 210 s [distinct from our measurement of $T_{1a}(^2H)$ = 33 s for the d_2 species]; however, $T_1(^2H)$ is reported to vary depending on the orientation of the sample.[61] These phenomena could be further investigated by variable-temperature (VT) $T_1(^2H)$ measurements of α-glycine-d_2.

E. ^{195}Pt experiments

Accurately measuring $T_1(^{195}Pt)$ presents a unique challenge in cases where the platinum CSA is large, which can result in patterns that span several thousands of ppm (i.e., pattern breadths of >500 kHz at fields of 9.4 T or higher). $Pt(NH_3)_4Cl_2{\cdot}H_2O$ is used as a test case herein with a UWNMR powder pattern that spans nearly 1 MHz at 14.1 T [an ideal pattern is shown in Fig. S1(d)]. Both BRAIN-CPT1 and WCPMG-IR experiments were conducted for this sample; with recycle delays of 30 s and 12 s, single sub-spectra were acquired in total experimental times of 144 min and 67 min,

respectively. The pattern bandwidth far exceeds the uniform excitation bandwidth of the probe used in these experiments; therefore, a variable offset cumulative spectra (VOCS) methodology was implemented[44,62,63] with three acquisitions at different transmitter offsets. Figure 5(a) shows the coadded dataset for a VOCS-BRAIN-CPT1 experiment executed at transmitter offsets of +119 kHz, −204 kHz, and −535 kHz with respect to $\nu_0(^{195}\text{Pt})$. The positive magnitude-processed spectra are shown as a function of delay time, τ, revealing the non-uniformity of longitudinal relaxation across isochromats for different τ values. This is easiest to see by the null point in the data (i.e., the point along the τ axis where the signal intensity approaches zero, as indicated by the dark blue contour), which appears roughly as a lop-sided normal distribution that is skewed heavily to the low-frequency side of the pattern. It is unlikely that this lop-sided intensity distribution originates from bandwidth limitations in probe excitation or detection since acquisitions at multiple offset frequencies have been performed; therefore, this is the possible evidence of T_1 anisotropy. The isochromats with the longest T_1 time constants are centered at ~−280 kHz [this region is denoted by * in Fig. 5(a)]. Interestingly, this occurs near the isotropic chemical shift of −2540 ppm or −327 kHz.[11] These factors suggest that fitting the integrated powder pattern intensities as a function of τ only gives information on the average value of T_1, while not providing an

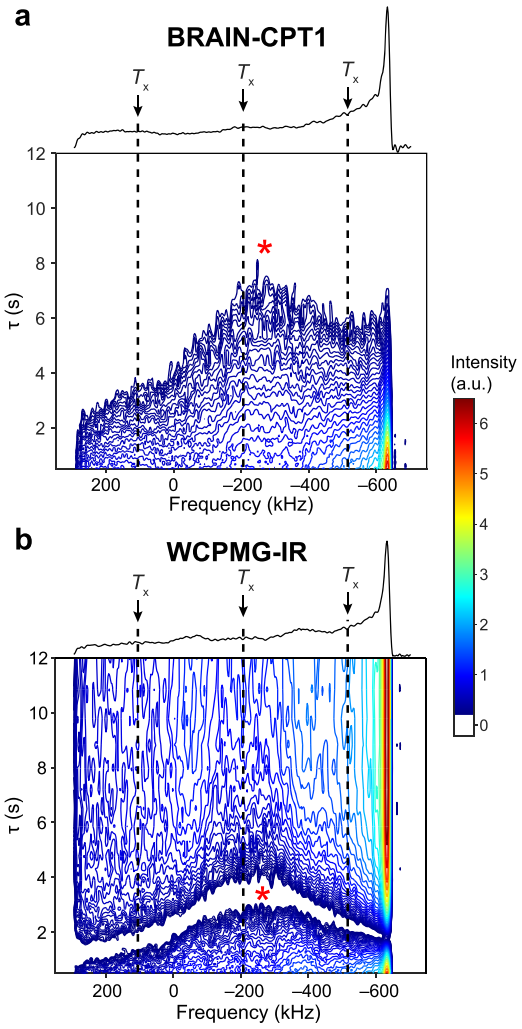

FIG. 5. ^{195}Pt NMR spectra of $Pt(NH_3)_4Cl_2{\cdot}H_2O$. (a) Spectra acquired with the BRAIN-CPT1 pulse sequence with the transmitter offsets at ~+119 kHz, −204 kHz, and −535 kHz (indicated by T_x) with respect to $\nu_0(^{195}\text{Pt})$. Resulting spectra acquired at each offset are coadded together. Positive magnitude contours of the powder patterns are shown as a function of the delay, τ. A single 1D spectrum from the experiment, taken from τ = 0, is shown as a projection on the frequency axis. (b) Spectra acquired with the WCPMG-IR pulse sequence using the same offsets and coaddition as in (a). In both cases, a region of interest is denoted by the red asterisks (*, see text for details).

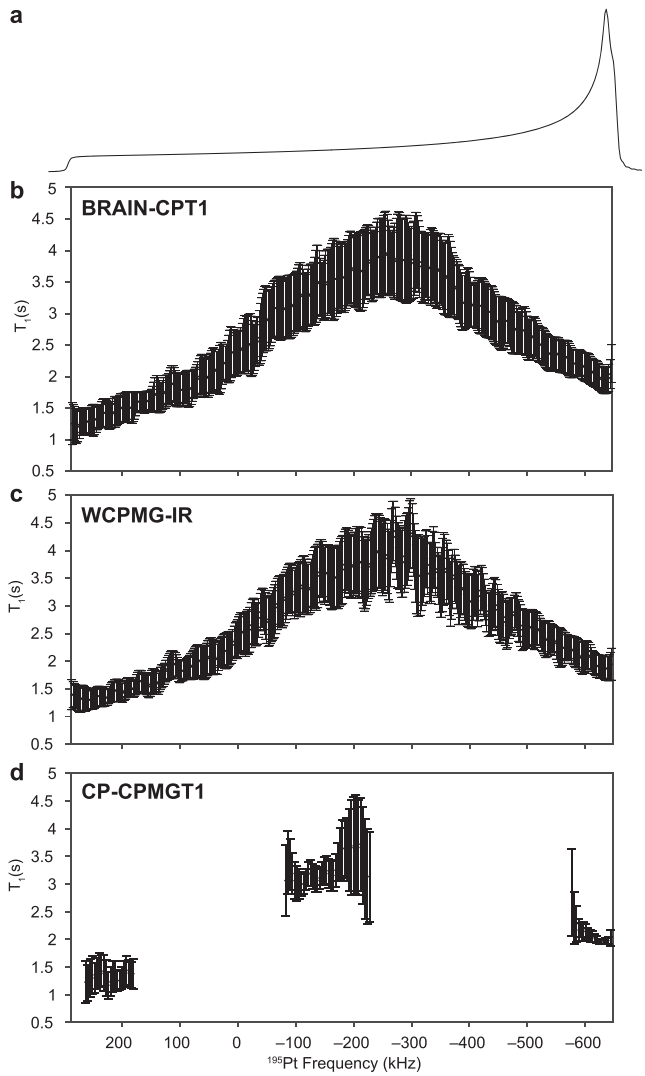

FIG. 6. (a) Simulated ^{195}Pt NMR spectrum of $Pt(NH_3)_4Cl_2{\cdot}H_2O$. Monoexponential fits of the spectral intensities across the powder pattern as a function of the delay, τ, for the (b) BRAIN-CPT1, (c) WCPMG-IR, and (d) CP-CPMGT1 experiments.

TABLE II. ^{195}Pt T_1 anisotropy measurements.

Frequency[a] (kHz)	Experiment	T_{1a} (s)	*RMSE*
+218	BRAIN-CPT1	1.4 ± 0.2	0.0382
	WCPMG-IR	1.4 ± 0.1	0.0560
	CP-CPMGT1	1.2 ± 0.3	0.0991
−131	BRAIN-CPT1	3.3 ± 0.5	0.0409
	WCPMG-IR	3.5 ± 0.5	0.0901
	CP-CPMGT1	3.1 ± 0.2	0.0468
−631	BRAIN-CPT1	1.9 ± 0.2	0.0276
	WCPMG-IR	1.9 ± 0.2	0.0529
	CP-CPMGT1	1.95 ± 0.04	0.0298

[a]The transmitter frequency is offset with respect to $\nu_0(^{195}\text{Pt})$, and T_{1a} is fit using the integrated intensity at the pattern acquired at that frequency.

accurate measure of the T_1 anisotropy; as such, a different form of analysis must be used (*vide infra*).

The VOCS-WCPMG-IR experiment was conducted in a similar manner [Fig. 5(b)] with the same three transmitter offsets as VOCS-BRAIN-CPT1. The coadded IR data reveal a similar distribution in longitudinal relaxation for different isochromats. The points along the τ axis where the null points occur differ from the VOCS-BRAIN-CPT1 data since the isochromats relax with a different exponential decay function during an IR-type of pulse sequence.

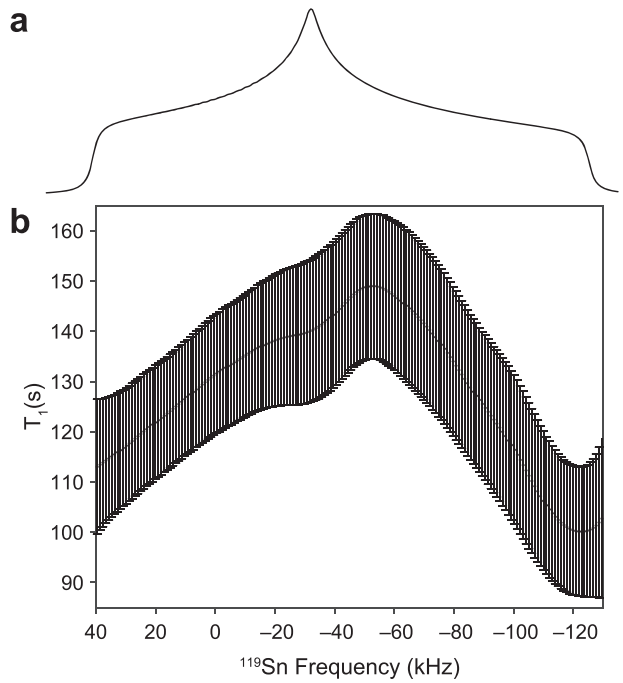

FIG. 7. (a) Simulated ^{119}Sn NMR spectrum of dibutyltin(IV) oxide. Monoexponential fits of the spectral intensities across the powder pattern as a function of the delay, τ, for the (b) BRAIN-CPT1 experiment.

Nonetheless, a similar distribution in the null points is observed and the isochromats with the longest T_1 constants occur in the same region as those from the VOCS-BRAIN-CPT1 experiment, again near the isotropic chemical shift [denoted by * in Fig. 5(b)].

F. T_1 anisotropy in CSA-dominated powder patterns

The evidence of T_1 anisotropy in ^{195}Pt experiments suggests that integrating over the entire pattern breadth may not be the most accurate way to measure T_1. Both ^{195}Pt relaxation datasets were fit with a monoexponential decay function using the spectral intensity corresponding to each individual frequency point, allowing for the fit of T_1 as a function of powder pattern frequency (*N.B.*: These

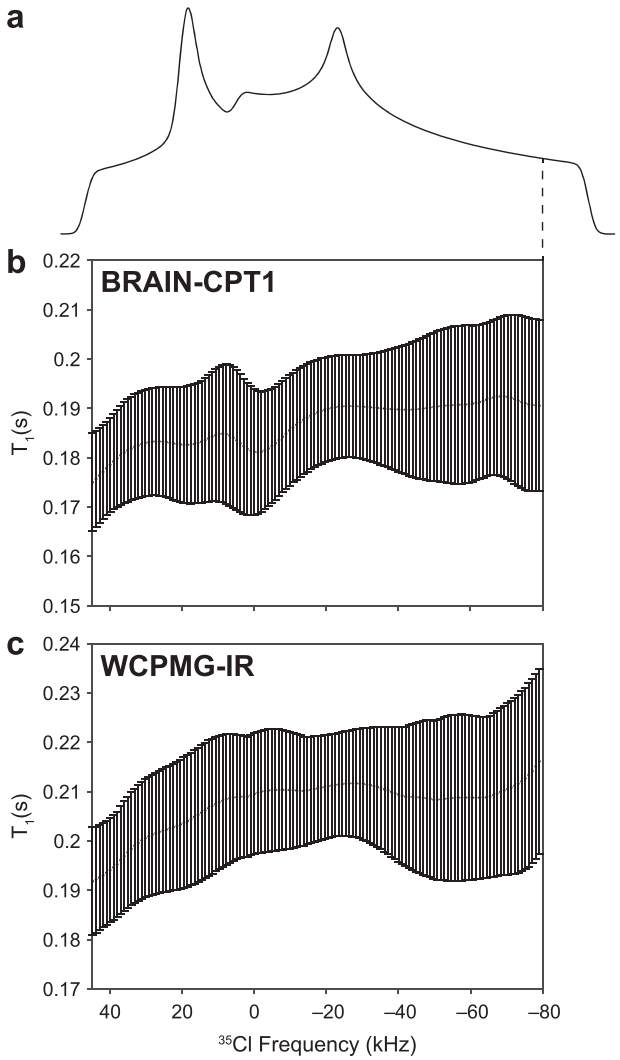

FIG. 8. (a) Simulated ^{35}Cl NMR spectrum of glycine HCl. Monoexponential fits of the spectral intensities across the powder pattern as a function of the delay, τ, for the (b) BRAIN-CPT1 and (c) WCPMG-IR experiments. The data are truncated on the low-frequency side of the powder pattern where the *RMSE* values increase significantly (the dashed line denotes where the data were truncated).

^{195}Pt data cannot be fit with a biexponential function). Figure 6(b) shows the fits for the coadded VOCS-BRAIN-CPT1 data from Fig. 5. The fitted T_1 values are plotted with their 95% confidence bounds as error bars with the smallest and longest T_1's being 1.2 ± 0.3 s and 4.0 ± 0.6 s, respectively [Fig. 6(b)]. The longest T_1 occurs at ~−308 kHz, which is close to the frequency of the isotropic shift (~−327 kHz). VOCS-WCPMG-IR measurements were conducted using the same conditions as BRAIN-CPT1, and the fits yield a very similar distribution of T_1 values [Fig. 6(c)] with the smallest and largest values of 1.3 ± 0.2 s and 4.4 ± 0.5 s, respectively, and the longest T_1 occurring at ~−270 kHz, again near the frequency of the isotropic shift. The large discrepancy between the smallest and longest T_1's outside of the error bounds confirms the orientation dependence of T_1. This observation of a T_1 anisotropy for static CSA-influenced powder patterns follows the second-rank Legendre polynomial orientation dependence observed by Pines *et al.* for ^{13}C CP-enhanced patterns of benzene,[64] where isochromats with tensor orientations described by the angle between δ_{33} and B_0 being near the magic angle (i.e., the isotropic shift) are associated with the highest T_1 values. These results can be confirmed using a pseudo-inverse Laplace transform (ILT) using Tikhonov regularization (Fig. S8); however, in the present work, the general implementation of this technique is limited due to the sensitivity to noisy data and the inability to assign statistical significance to the results (Fig. S8).[47,65]

The CP-CPMGT1 experiment was run on this sample to verify that BRAIN-CP does not encode any artifacts in the T_1 anisotropy measurement. CP-CPMGT1 is far too narrow-banded to enable acquisition of the entire powder pattern (*vide supra*); therefore, the experiment was executed at three distinct transmitter offsets of +218 kHz, −131 kHz, and −631 kHz with respect to ν_0(^{195}Pt) to confirm the presence of T_1 anisotropy [Fig. 6(d)]. The sequence uniformly excites and refocuses isochromats over a bandwidth of ~70 kHz in this case; therefore, corresponding T_1 fits are only conducted over those uniform regions. The overall distribution of these data agrees with the BRAIN-CPT1 and WCPMG-IR measurements, and specifically, the fitted T_1's at the same frequencies as the transmitter offsets for the CP-CPMGT1 experiment agree well between all the experiments (Table II). Therefore, the T_1 anisotropy can be reliably measured using both BRAIN-CPT1 and WCPMG-IR.

This encouraged us re-examine the ^{119}Sn NMR data of dibutyltin(IV) oxide (cf. Fig. 2), which was subjected to the same analysis (Fig. 7). In this case, biexponential fits are better suited for these data; however, the frequency-dependent fit was conducted with a monoexponential function for simplicity and still provides high correlation with the data (*vide supra*). T_1's vary between 100 ± 10 s and 149 ± 10 s with a mean of 128 s, in comparison to the monoexponential T_1 measured from integrating the powder pattern, which is 131 ± 7 s. This discrepancy outside the bounds of error again confirms the presence of T_1 anisotropy. The relative amount of error can vary depending on the amount of noise in the experimental dataset. In this case, the longest T_1 occurs at ~−52 kHz, where the isotropic shift is reported as −198 ppm = −44 kHz for this system.[48] This suggests a T_1 anisotropy akin to observations for ^{195}Pt experiments and earlier work by Pines *et al.*, though the mechanism in each case may be different.[64]

G. T_1 anisotropy in quadrupolar powder patterns

The orientation-dependent monoexponential fitting was conducted on the ^{35}Cl NMR data of glycine HCl (cf. Fig. 3). Measurements with BRAIN-CPT1 [Fig. 8(b)] and WCPMG-IR [Fig. 8(c)]

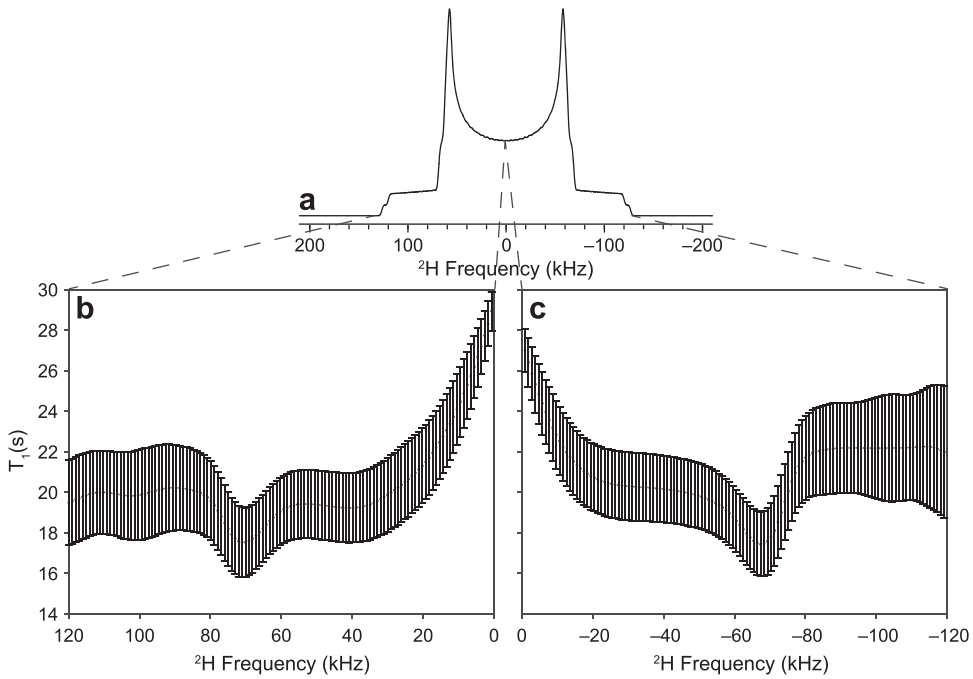

FIG. 9. (a) Simulated ^{2}H NMR spectrum of α-glycine-d_2. Monoexponential fits of the (b) positive- and (c) negative-spectral intensities across the powder pattern as a function of the delay, τ, for the BRAIN-CPT1 experiments.

reveal no distinct differences between T_1 outside the bounds of error, suggesting no discernable T_1 anisotropy for this sample. These orientation-dependent measurements also agree with the monoexponential T_1's measured from pattern integration within the bounds of error, where 187 ± 6 ms and 210 ± 7 ms were measured for BRAIN-CPT1 and WCPMG-IR, respectively. The absence of observable T_1 anisotropy is consistent with previous orientation-dependent T_1 measurements for half-integer quadrupolar nuclei.[6]

The same fitting procedure was applied to the ^{2}H NMR data of α-glycine-d_2 (cf. Fig. 4). T_1 fits from the high-frequency half of the pattern vary from 19 ± 2 s to 29 ± 1 s [Fig. 9(b)] and those from the low-frequency half vary from 22 ± 3 s to 27 ± 1 s [Fig. 9(c)] in comparison to their integrated monoexponential fits of 20.1 ± 0.9 s and 20.4 ± 0.9 s, respectively. The lower and upper limits of the T_1 values are well separated, each lying well outside of the bounds of uncertainty of the other, and, therefore, suggesting a T_1 anisotropy. The longest T_1 is found to occur at $\nu_0(^2\mathrm{H})$, where the quadrupolar frequency is zero, and then T_1 becomes shorter for non-zero values. This variation of T_1 agrees with observations and theoretical models of T_1 anisotropy in wideline ^{2}H spectra from the work of Griffin *et al.*[8,26,66]

IV. CONCLUSIONS

BRAIN-CPT1 and WCPMG-IR are shown to be efficient and reliable methods for measuring T_1 constants for powder patterns of spin-1/2 nuclei influenced by large CSAs, spin-3/2 nuclei affected by large SOQI's, and spin-1 nuclei dominated by FOQI's. These methods are superior for measuring T_1's of static UWNMR spectra in comparison to those using rectangular pulses of constant amplitude and phase. T_1 measurements under static conditions may be closer to the ground-truth T_1 than in MAS experiments, especially in cases where spin diffusion can occur between heteronuclear or homonuclear spin pairs due to energy level crossings over the course of a rotor cycle that can influence T_1.[50,67,68] CP-based sequences allow for the rapid measurement of $T_1(S)$ constants in cases where CP offers signal enhancement and/or $T_1(^1\mathrm{H}) < T_1(S)$. For static UWNMR spectra with high S/N, it is possible to obtain very good fits of T_1 data using both monoexponential and biexponential relaxation formulae (the exception is the ^{195}Pt data, which can be adequately fit considering only monoexponential decay). The mechanisms giving rise to biexponential decay are currently unknown and can only be speculated upon since there are relatively few investigations of this kind for static SSNMR in the literature. Possible relaxation mechanisms include dipolar and CSA mechanisms in experiments on spin-1/2 nuclei and competing dipolar and quadrupolar mechanisms for quadrupolar nuclei (cross relaxation effects can be ruled out for the cases investigated herein); further study into these phenomena is underway in our group, and specific attributions of the mechanisms and their relative contributions are beyond the scope of the present work. T_1 anisotropy is observed in the cases of ^{119}Sn, ^{2}H, and ^{195}Pt NMR. T_1 anisotropy, especially in spin-1/2 nuclei, can manifest differently depending on the local structure about the observed nucleus, and such information would typically be lost under MAS conditions.[5,69] It is possible that VT T_1 anisotropy measurements could aid in structural characterization and dynamics studies. Having established what appear to be reliable methods for measuring both the average T_1 values and ranges of anisotropic T_1 values, we plan to apply these methods in future UWNMR studies to investigate the relaxation mechanisms that contribute to biexponential and anisotropic longitudinal relaxation behavior, respectively. These robust and versatile sequences may prove useful for measuring T_1 constants for a wide variety of spin-1/2 and quadrupolar nuclei across the periodic table as well as offering the potential to simultaneously measure T_1 and T_2^{eff} time constants and deconvolute contributions from distinct relaxation mechanisms.

SUPPLEMENTARY MATERIAL

See the supplementary material for additional simulations, experiments, and processing details.

ACKNOWLEDGMENTS

R.W.S. and A.R.A. would like to thank the National Science Foundation Chemical Measurement and Imaging Program with partial co-funding from the Solid State and Materials Chemistry Program (Grant No. NSF-2003854) for supporting this work as well as The Florida State University and the National High Magnetic Field Laboratory (NHMFL), which is funded by the National Science Foundation Cooperative Agreement (Grant No. DMR-1644779) and by the State of Florida. R.W.S. is also grateful for early funding of this work from the Natural Sciences and Engineering Research Council of Canada (NSERC, Grant No. RGPIN-2016_06642 Discovery Grant). K.J.H. is grateful for financial support through the Louisiana Board of Regents [LEQSF(2019-22)-RD-A-17].

DATA AVAILABILITY

All MATLAB code, simulation input files, pulse programs, and NMR datasets are available from the corresponding author upon reasonable request.

REFERENCES

[1] A. Abragam, *The Principles of Nuclear Magnetism* (Oxford Science Publications, Oxford, 1961).
[2] P. A. Beckmann, Phys. Rep. **171**, 85 (1988).
[3] R. E. Wasylishen, *NMR Spectroscopy Techniques* (Marcel Dekker, Inc., New York, 1996), pp. 105–144.
[4] R. W. Schurko, Acc. Chem. Res. **46**, 1985 (2013).
[5] M. G. Gibby, A. Pines, and J. S. Waugh, Chem. Phys. Lett. **16**, 296 (1972).
[6] E. R. Andrew, K. M. Swanson, and B. R. Williams, Proc. Phys. Soc. **77**, 36 (1961).
[7] D. A. Torchia and A. Szabo, J. Magn. Reson. **49**, 107 (1982).
[8] R. J. Wittebort, E. T. Olejniczak, and R. G. Griffin, J. Chem. Phys. **86**, 5411 (1987).
[9] C. Dybowski and G. Neue, Prog. Nucl. Magn. Reson. Spectrosc. **41**, 153 (2002).
[10] P. Amornsakchai, D. C. Apperley, R. K. Harris, P. Hodgkinson, and P. C. Waterfield, Solid State Nucl. Magn. Reson. **26**, 160 (2004).
[11] B. E. G. Lucier, K. E. Johnston, W. Xu, J. C. Hanson, S. D. Senanayake, S. Yao, M. W. Bourassa, M. Srebro, J. Autschbach, and R. W. Schurko, J. Am. Chem. Soc. **136**, 1333 (2014).
[12] A. Sebald, *NMR Basic Principles and Progress* (Spring-Verlag, Berlin, Heidelberg, 1994), pp. 91–131.
[13] P. A. Beckmann, S. Bai, A. J. Vega, and C. Dybowski, Phys. Rev. B **74**, 214421 (2006).
[14] A. J. Vega, P. A. Beckmann, S. Bai, and C. Dybowski, Phys. Rev. B **74**, 214420 (2006).

[15]J. B. Grutzner, K. W. Stewart, R. E. Wasylishen, M. D. Lumsden, C. Dybowski, and P. A. Beckmann, J. Am. Chem. Soc. **123**, 7094 (2001).
[16]A. Naito, S. Ganapathy, K. Akasaka, and C. A. McDowell, J. Magn. Reson. **54**, 226 (1983).
[17]J. S. Frye, Concepts Magn. Reson. **1**, 27 (1989).
[18]K. Akasaka, S. Ganapathy, C. A. McDowell, and A. Naito, J. Chem. Phys. **78**, 3567 (1983).
[19]E. Carignani, S. Borsacchi, and M. Geppi, J. Phys. Chem. A **115**, 8783 (2011).
[20]J. Zhou, R. Fu, J. Z. Hu, L. Li, and C. Ye, Solid State Nucl. Magn. Reson. **7**, 291 (1997).
[21]Y. L. Wang, H. R. Tang, and P. S. Belton, J. Phys. Chem. B **106**, 12834 (2002).
[22]H. He, J. Teixeira Dias, J. Foulkes, and J. Klinowski, Phys. Chem. Chem. Phys. **2**, 2651 (2000).
[23]D. C. Apperley, A. F. Markwell, I. Frantsuzov, A. J. Ilott, R. K. Harris, and P. Hodgkinson, Phys. Chem. Chem. Phys. **15**, 6422 (2013).
[24]R. E. Taylor, N. Chim, and C. Dybowski, J. Mol. Struct. **794**, 133 (2006).
[25]J. C. Williams and A. E. McDermott, J. Phys. Chem. **97**, 12393 (1993).
[26]D. J. Siminovitch, M. J. Ruocco, E. T. Olejniczak, S. K. Das Gupta, and R. G. Griffin, Biophys. J. **54**, 373 (1988).
[27]H. W. Spiess, J. Chem. Phys. **72**, 6755 (1980).
[28]D. A. Torchia, J. Magn. Reson. **30**, 613 (1978).
[29]E. O. Stejskal and J. Schaefer, J. Magn. Reson. **18**, 560 (1975).
[30]I. Solomon, Phys. Rev. **99**, 559 (1955).
[31]J. P. Yesinowski, J. Magn. Reson. **180**, 147 (2006).
[32]J. P. Yesinowski, J. Magn. Reson. **252**, 135 (2015).
[33]A. Venkatesh, M. P. Hanrahan, and A. J. Rossini, Solid State Nucl. Magn. Reson. **84**, 171 (2017).
[34]M. Makrinich and A. Goldbourt, Chem. Commun. **55**, 5643 (2019).
[35]R. W. Schurko, *Encyclopedia of Magnetic Resonance* (John Wiley & Sons, Ltd., Chichester, UK, 2011), pp. 77–93.
[36]A. Medek, J. S. Harwood, and L. Frydman, J. Am. Chem. Soc. **117**, 12779 (1995).
[37]Z. Gan, J. Am. Chem. Soc. **122**, 3242 (2000).
[38]L. A. O'Dell and R. W. Schurko, Chem. Phys. Lett. **464**, 97 (2008).
[39]K. J. Harris, S. L. Veinberg, C. R. Mireault, A. Lupulescu, L. Frydman, and R. W. Schurko, Chem. - Eur. J. **19**, 16469 (2013).
[40]È. Kupce and R. Freeman, J. Magn. Reson., Ser. A **117**, 246 (1995).
[41]F. H. Larsen, H. J. Jakobsen, P. D. Ellis, and N. C. Nielsen, J. Magn. Reson. **131**, 144 (1998).
[42]F. H. Larsen, H. J. Jakobsen, P. D. Ellis, and N. C. Nielsen, Chem. Phys. Lett. **292**, 467 (1998).
[43]I. Hung and Z. Gan, J. Magn. Reson. **204**, 256 (2010).
[44]A. R. Altenhof, M. J. Jaroszewicz, A. W. Lindquist, L. D. D. Foster, S. L. Veinberg, and R. W. Schurko, J. Phys. Chem. C **124**, 14730 (2020).
[45]R. Bhattacharyya and L. Frydman, J. Chem. Phys. **127**, 194503 (2007).
[46]S. L. Veinberg, Z. W. Friedl, K. J. Harris, L. A. O'Dell, and R. W. Schurko, CrystEngComm **17**, 5225 (2015).
[47]M. J. Jaroszewicz, L. Frydman, and R. W. Schurko, J. Phys. Chem. A **121**, 51 (2017).
[48]K. J. Harris, A. Lupulescu, B. E. G. Lucier, L. Frydman, and R. W. Schurko, J. Magn. Reson. **224**, 38 (2012).
[49]D. L. Bryce, G. D. Sward, and S. Adiga, J. Am. Chem. Soc. **128**, 2121 (2006).
[50]K. Takegoshi, M. Ito, and T. Terao, Chem. Phys. Lett. **260**, 159 (1996).
[51]M. Bak, J. T. Rasmussen, and N. C. Nielsen, J. Magn. Reson. **213**, 366 (2011).
[52]Y. Kusaka, T. Hasegawa, and H. Kaji, J. Phys. Chem. A **123**, 10333 (2019).
[53]A. M. Namespetra, D. A. Hirsh, M. P. Hildebrand, A. R. Sandre, H. Hamaed, J. M. Rawson, and R. W. Schurko, CrystEngComm **18**, 6213 (2016).
[54]D. A. Hirsh, A. J. Rossini, L. Emsley, and R. W. Schurko, Phys. Chem. Chem. Phys. **18**, 25893 (2016).
[55]A. R. Altenhof, A. W. Lindquist, L. D. D. Foster, S. T. Holmes, and R. W. Schurko, J. Magn. Reson. **309**, 106612 (2019).
[56]J. Koppe and M. R. Hansen, J. Phys. Chem. A **124**, 4314 (2020).
[57]S. L. Veinberg, A. W. Lindquist, M. J. Jaroszewicz, and R. W. Schurko, Solid State Nucl. Magn. Reson. **84**, 45 (2016).
[58]T. Mizuno, K. Takegoshi, and T. Terao, J. Chem. Phys. **122**, 084322 (2005).
[59]S. Wi, R. W. Schurko, and L. Frydman, Solid State Nucl. Magn. Reson. **94**, 31 (2018).
[60]L. A. O'Dell and R. W. Schurko, J. Am. Chem. Soc. **131**, 6658 (2009).
[61]C. Müller, W. Schajor, H. Zimmermann, and U. Haeberlen, J. Magn. Reson. **56**, 235 (1984).
[62]L. A. O'Dell, A. J. Rossini, and R. W. Schurko, Chem. Phys. Lett. **468**, 330 (2009).
[63]D. Massiot, I. Farnan, N. Gautier, D. Trumeau, A. Trokiner, and J. P. Coutures, Solid State Nucl. Magn. Reson. **4**, 241 (1995).
[64]A. Pines, M. G. Gibby, and J. S. Waugh, J. Chem. Phys. **59**, 569 (1973).
[65]A. Lupulescu, M. Kotecha, and L. Frydman, J. Am. Chem. Soc. **125**, 3376 (2003).
[66]J. R. Long, R. Ebelhäuser, and R. G. Griffin, J. Phys. Chem. A **101**, 988 (1997).
[67]D. E. Woessner and H. S. Gutowsky, J. Chem. Phys. **29**, 804 (1958).
[68]J. F. J. M. Pourquié and R. A. Wind, Phys. Lett. A **55**, 347 (1976).
[69]A. Pines, M. G. Gibby, and J. S. Waugh, J. Chem. Phys. **56**, 1776 (1972).